Journal of Hydrology 628 (2024) 130525

Contents lists available at ScienceDirect

Journal of Hydrology

journal homepage: www.elsevier.com/locate/jhydrol

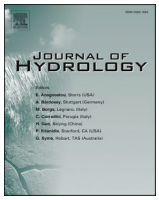

Research papers

Separating impacts of storm characteristics and mitigation activities on suspended sediment: Implications for sampling to evaluate mitigation success

T.W. Biggs [a,*], A.T. Messina [a,b], S.H. Rice [c], M.C. Hattori [d], H. McMillan [a]

[a] Department of Geography, San Diego State University, San Diego, CA, 92182, USA
[b] WSP USA, San Diego, CA 92123, USA
[c] National Oceanic and Atmospheric Administration, USA
[d] University of Hawai'i, Manoa, USA

ARTICLE INFO

Keywords:
Sediment load
Mitigation
Land based sources of pollution
Best management practices
Coral reefs

ABSTRACT

Mitigation activities are often implemented to reduce anthropogenic sediment loads to sensitive ecosystems, including coral reefs, but effectiveness is rarely documented due to a lack of pre-mitigation data and to the difficulty of separating the impacts of mitigation from those of storm size and intra- and inter-storm variability. Here we present a method using stormwise metrics to quantify the effectiveness of a sediment mitigation project in American Samoa, where an aggregate quarry covering <1 % of a small watershed (drainage area 1.8 km^2) generated approximately half of the annual suspended sediment load to the coast. Rainfall, runoff, turbidity and suspended sediment concentrations (SSC, mg L^{-1}), yield (SSY, tons km^{-2} per unit time) and loads (SSL, tons per unit time) were monitored periodically over a five-year period upstream and downstream of the quarry. Mitigation included revegetation and placement of gravel on roads and processing platforms followed by installation of retention ponds. Storms were identified using automated storm separation, and a simple regression model using maximum area-normalized storm discharge (Q_{max}) estimated SSC, SSY and SSL for each mitigation stage (post-gravel, post-ponds) for a reference storm sequence. Regression parameters, and SSL and SSC for the reference storm sequence were calculated for a range of storm separation parameters. Monte Carlo sampling of the regression errors was used to calculate a mean and standard deviation of SSL and its change following mitigation. SSC was nearly 100x higher during large storms than during small storms, demonstrating the need to account for storm size to detect impacts of mitigation. After mitigation, SSL downstream of the quarry decreased by 63–82 % for all storms and by 88–92 % for small storms, and SSY downstream of the quarry was similar to SSY from the forested watershed upstream. Mitigation of sediment loads can target a small fraction of a watershed area that accounts for the majority of the human impact. Combining stormwise metrics with simple regression modeling and uncertainty analysis is a simple and novel way to detect and quantify the effectiveness of mitigation activities on sediment loads.

1. Introduction

Land-based sources of pollution (LBSP) can stress aquatic and marine ecosystems in receiving waters. In the coastal tropics, increased sediment loads from LBSP can harm coral reefs by increasing turbidity, which interferes with photosynthesis, and by sedimentation on coral (Fabricius, 2005; Storlazzi et al., 2015). Mitigation activities are often proposed (Oleson et al., 2017) and implemented to reduce sediment loads (mass per time) to receiving water bodies (Mainstone et al., 2008), including from agriculture, mining, and urban construction. The effectiveness of mitigation activities, in particular the effectiveness of different stages and types of mitigation, is rarely quantified due to a lack of pre-mitigation (baseline) data, and to lack of funding for continued monitoring following mitigation (Kondolf, 1998; Rickson, 2014). Resources and funding are limited and often directed at further mitigation rather than additional monitoring. The appropriate goal for post-mitigation concentrations or loads is also difficult to identify, particularly if the pre-disturbance background loading rates are not known

* Corresponding author.
E-mail address: tbiggs@sdsu.edu (T.W. Biggs).

https://doi.org/10.1016/j.jhydrol.2023.130525
Received 23 January 2023; Received in revised form 23 August 2023; Accepted 2 November 2023
Available online 22 November 2023

(Rickson, 2014).

Several metrics are used to quantity sediment in streams, including suspended sediment concentrations (SSC, mg L^{-1}), yields (SSY, tons km^{-2} per time) and loads (SSL, tons per time). SSL is a key metric in watershed sediment budgets and is used by managers and policy makers. SSY (SSL divided by watershed area) facilitates comparison of sediment loads from different streams, controlling for watershed area. Quantification of the effectiveness of mitigation activities using these three sediment metrics is further complicated by their extreme spatial and temporal variability over multiple spatial and temporal scales (Morehead et al., 2003). Instantaneous SSC, SSY and SSL are non-linear functions of discharge, can differ on the rising and falling limbs of storm hydrographs (hysteresis), and depend on the time between storms (Walling and Webb, 1982). Interannual variability of rainfall amount,

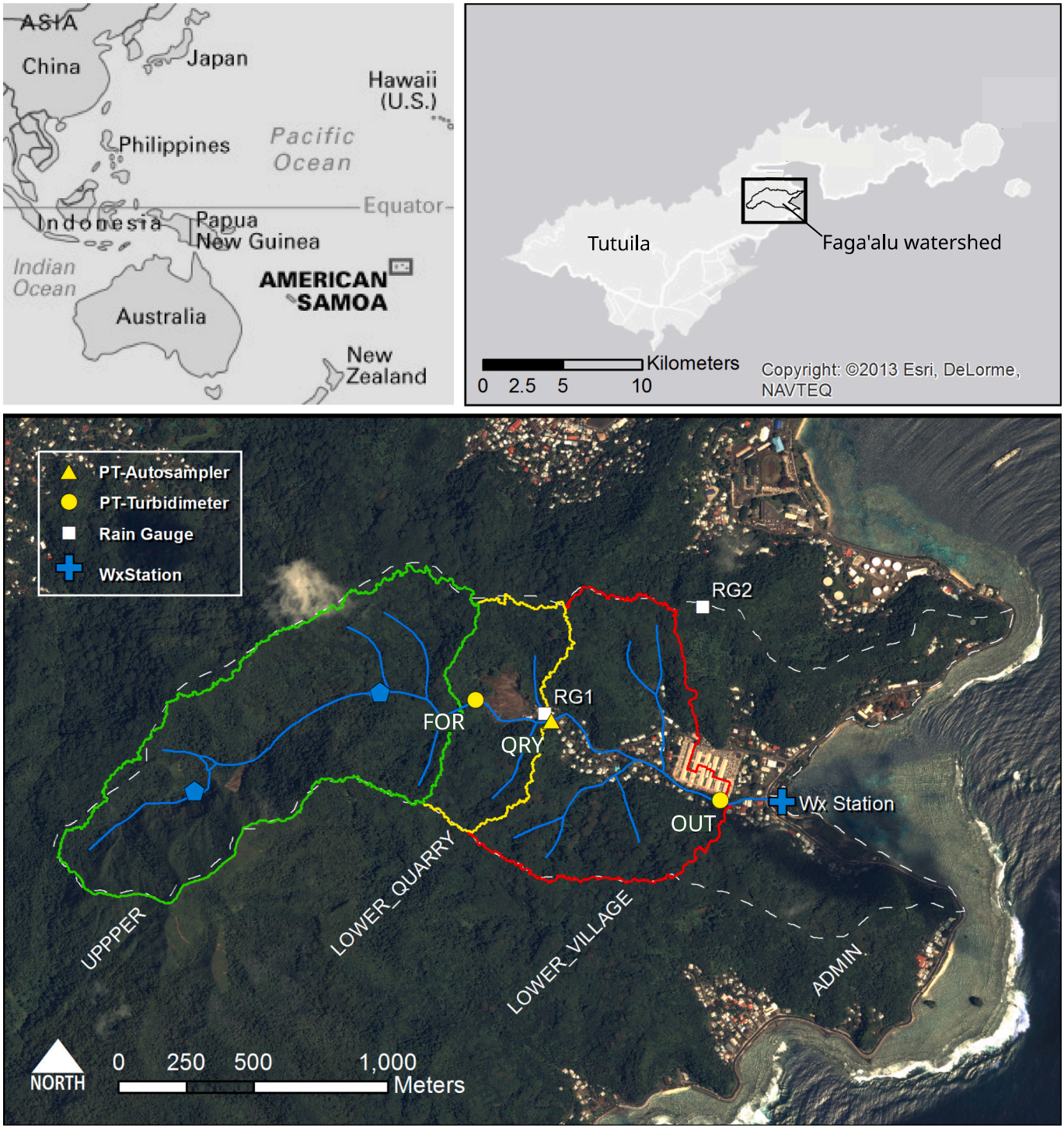

Fig. 1. Map of the study watershed and sampling locations. Water samples and discharge measurement were made at FOR and QRY. Rainfall data are from RG1. UPPER green polyline is the watershed draining to FOR. Yellow polyline is the subwatershed that drains to QRY, red polyline (LOWER_VILLAGE) is the subwatershed draining to the outlet point (OUT), and dashed white line (ADMIN) is the area draining to Faga'alu Bay. Blue pentagons in the upper watershed indicate small reservoirs. The weather station (Wx_station) was not used in this study. (For interpretation of the references to colour in this figure legend, the reader is referred to the web version of this article.)

timing, and sequence can result in large interannual variability in sediment loads (Inman and Jenkins, 1999), complicating the use of annual loads for mitigation assessment. The effectiveness of mitigation may also depend on storm size: small storms may show a larger percentage impact of mitigation on loads than large storms due to the finite capacity of mitigation activities to intercept or reduce loads, to the design of mitigation for a specified target storm size, and to large loads from other contributing areas during large events. Stormwise sediment metrics may be more predictable than instantaneous values, since intra-storm hysteresis is eliminated. Hydrological storm metrics, such as rainfall magnitude and intensity, storm runoff, and maximum storm discharge, can be robust predictors of stormwise SSY (Duvert et al., 2012; Messina and Biggs, 2016), suggesting that if data on stormwise SSC, SSY and/or SSL are available for pre-mitigation conditions, or where a watershed with minimal disturbance is available for comparison, mitigation effectiveness can be quantified.

The objectives of this paper are to 1) quantify the impacts of storm size and mitigation activities on stormwise SSC, SSY and SSL, and 2) identify the impact of different stages of mitigation on SSC and SSL, controlling for differences in storm size among monitoring periods. The case study is a small watershed (1.8 km^2) in American Samoa, where an aggregate quarry was an important sediment source and was the focus of mitigation activities in 2013–2015. Stream discharge, turbidity, and SSC were measured upstream and downstream of the quarry during field campaigns spanning five years (2012–2016). The study builds on previous work (Messina and Biggs, 2016) that documented that the quarry covers<1 % of the watershed area but contributes up to half of the SSL. The analysis includes data before, during and after mitigation activities at the quarry, which included placement of gravel on unpaved surfaces followed by installation of retention ponds. The implications for sediment mitigation strategies and documentation of their effectiveness are discussed, and a workflow is presented for use elsewhere. The main research questions include:

RQ1: How does storm size impact SSC and SSY in different mitigation stages?

RQ2: How do turbidity, SSC, SSY and SSL compare upstream and downstream of the quarry following mitigation, during baseflow and stormflow, for a range of storm sizes?

RQ3: Did mitigation activities reduce SSC and SSL downstream of the quarry over time, controlling for differences in the storm size distribution among monitored periods?

2. Study area

2.1. Physiographic features

Faga'alu watershed, on the island of Tutuila in American Samoa (14S, 170 W), drains a total of 1.8 km^2 where it discharges to the ocean, including a forested upper watershed and a lower subwatershed that has an aggregate quarry and a village (Fig. 1). Faga'alu stream discharges to Faga'alu Bay and its coral reef, parts of which are impacted by excess sedimentation (Holst-Rice et al., 2016). In 2012, the watershed was selected as a Priority Watershed for conservation and remediation by the US Coral Reef Task Force (Holst-Rice et al., 2016).

Annual precipitation in the watershed varies from 3,800 mm on the coast to 6,350 mm at the highest point (653 m.a.s.l.) (Messina and Biggs, 2016). Mean air temperatures are high (28 °C) year-round (Shuler et al, 2020). A drier season from June through September accounts for 33 % of the days of the year but 25 % of annual precipitation, though large storms can occur year-round. Tropical cyclones hit American Samoa approximately once every 2.5 years (Patterson, 1981), though 2010–2015 had below average activity (Marra and Kruk, 2017). Streamflow in Faga'alu is flashy, and baseflow accounts for only 39 % of annual streamflow (Shuler et al, 2020).

The rock underlying Faga'alu is basalt formed from shield volcanoes, which is similar to other volcanic islands in the Pacific (McDougall, 1987). Mean slope in the watershed is 0.53 m/m with 653 m of relief. The valley bottom has a wedge of marine and terrestrial alluvium that extends up to 1 km from the coast (Shuler et al, 2020). Soils on the hillsides include rock outcrops (15 %) and shallow (20–150 cm) silty clay to clay loams (Lithic Hapludolls), while lowland soils are deep (>150 cm) stony silty clay loams, and valley bottoms have silty clay and fine sandy loams (Nakamura, 1984). Shallow landslides are common.

Land cover in the watershed defined by the outlet to the ocean is mostly undisturbed tropical rainforest and shrubs (95 % of the watershed area) with small areas of village and developed open space (4 %), the quarry (1.6 ha, 1 %), and small agricultural plots (0.3 %) (Messina and Biggs, 2016). The upper forested watershed (drainage area 0.9 km^2) has some abandoned reservoirs built in the early 1900 s, but the sediment that has accumulated in the reservoir is largely coarse gravel and cobble, suggesting that fine sediment is washload and has not accumulated in the reservoirs.

2.2. Aggregate quarry and mitigation measures

The aggregate quarry lies upstream of the village and was established in the 1960 s. The quarry has access roads, an active blast face, excavation platform, piles of processed and pre-processed aggregate, and upper and lower platforms for processing (Fig. 2). The southern boundary of the quarry is close to the stream with a very narrow vegetated buffer (<5 m). Prior to mitigation, runoff from the quarry entered directly into the stream via two small (<30 cm wide) channels that cut through the buffer. In 2011, silt-fences and two small settling ponds were installed at the base of the quarry, but the mitigation was inadequate to accommodate the sediment load and the ponds filled early in the rainy season (Horsley Witten Group Inc, 2013). Between 2012 and 2014, additional mitigation activities were performed, including revegetation of tailing piles, diversion of a groundwater seep that flowed through the quarry, placement of gravel (~1–4 cm diameter) on the unpaved roads and processing platforms, and construction of retention ponds (Fig. 3, Fig. 4, Table 1). The capacity of the ponds is 20,768 ft^3 (588 m^3) and 11,305 ft^3 (320 m^3), for a total of 908 m^3 (Horsley Witten Group, 2014, cited in Holst-Rice et al., 2016). Assuming a sediment bulk density of 1.6 tons m^{-3}, the combined pond storage capacity is 1450 tons. Here, we define three mitigation stages: pre-mitigation, post-gravel, and post-ponds (Fig. 5). The post-gravel period includes the impact of both the seep diversion and gravel placement.

3. Methods

The literature uses several different terms to describe sediment transport by rivers, and terms vary among sources. We use the term suspended sediment load (SSL) to indicate the mass (tons) of suspended sediment discharged by a stream past a particular point over a given period of time, where the time period could range from seconds to years (Syvitski et al., 2005) or storm event or monitoring period. Suspended sediment yield (SSY, tons km^{-2} per time) is the area-normalized load per a given period of time (Milliman and Meade, 1983) or storm event (Duvert et al., 2012). Others have referred to the sediment discharge (mass per time) as the yield, and the area-normalized sediment discharge as the specific sediment yield (Walling and Webb, 1996; Messina and Biggs, 2016). Here we use load and yield as defined by Syvitski et al. (2005), Milliman and Meade (1983), and Duvert et al (2012).

The methods have three main components (see workflow in Fig. S1): discharge, turbidity and sediment monitoring (3.1), storm identification using automated stormflow separation and regression modeling of stormwise SSC and SSY as functions of area-normalized storm maximum discharge (Q_{max}, m^3 s^{-1} km^{-2}) (RQ1, Section 3.2), and mitigation impact assessment and uncertainty analysis (RQ2 and RQ3, Section 3.3). For mitigation assessment, turbidity, SSC, SSY and SSL were first compared upstream and downstream of the quarry in the post-

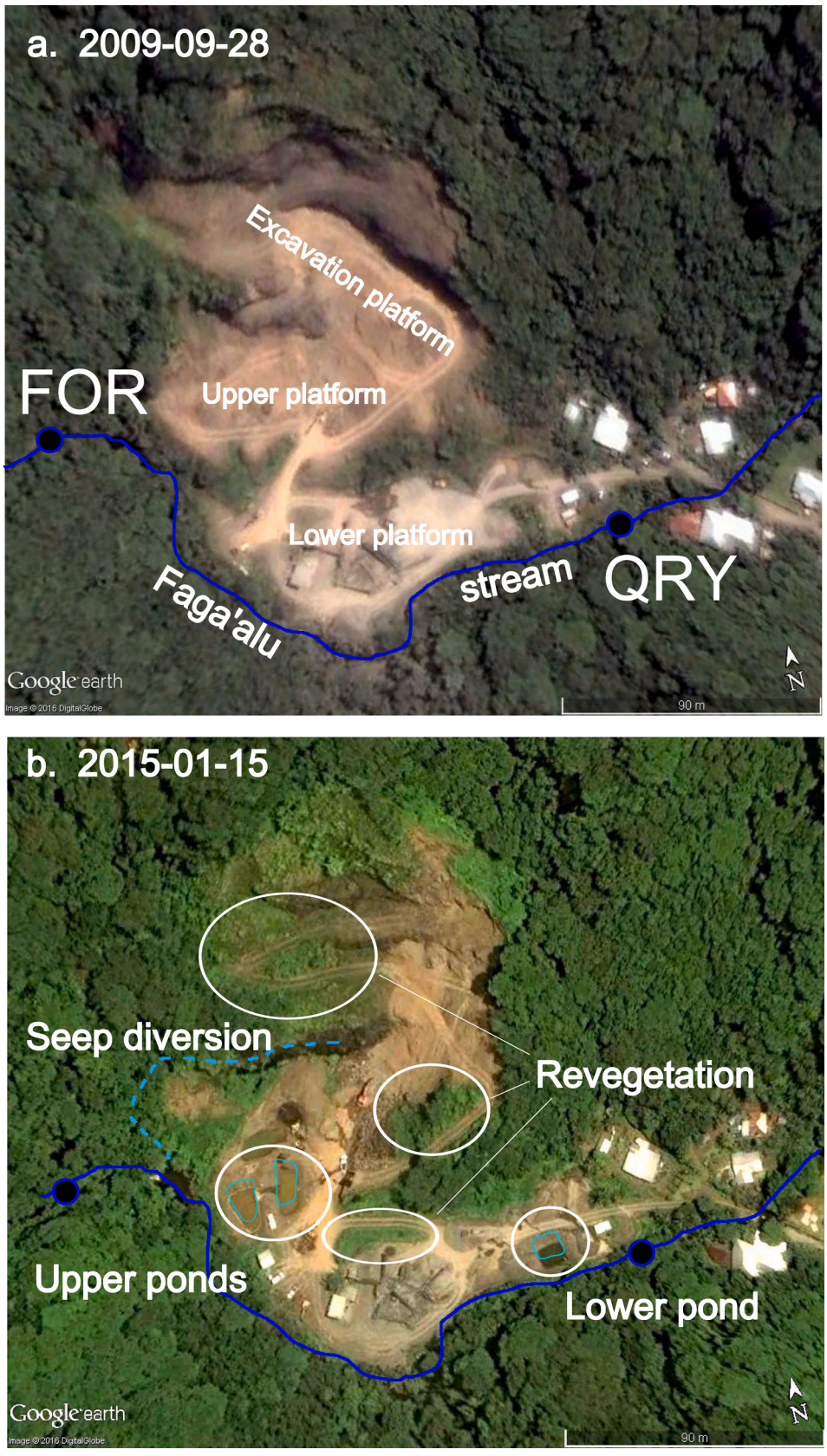

Fig. 2. Aerial photos of the quarry indicating the sampling points on the stream (FOR and QRY) and surface conditions a) before mitigation in 2009, including the excavation platform, upper processing platform ("upper platform") and lower processing platform ("lower platform") and b) after mitigation activities, including groundwater seep diversion, revegetation, and sediment retention ponds.

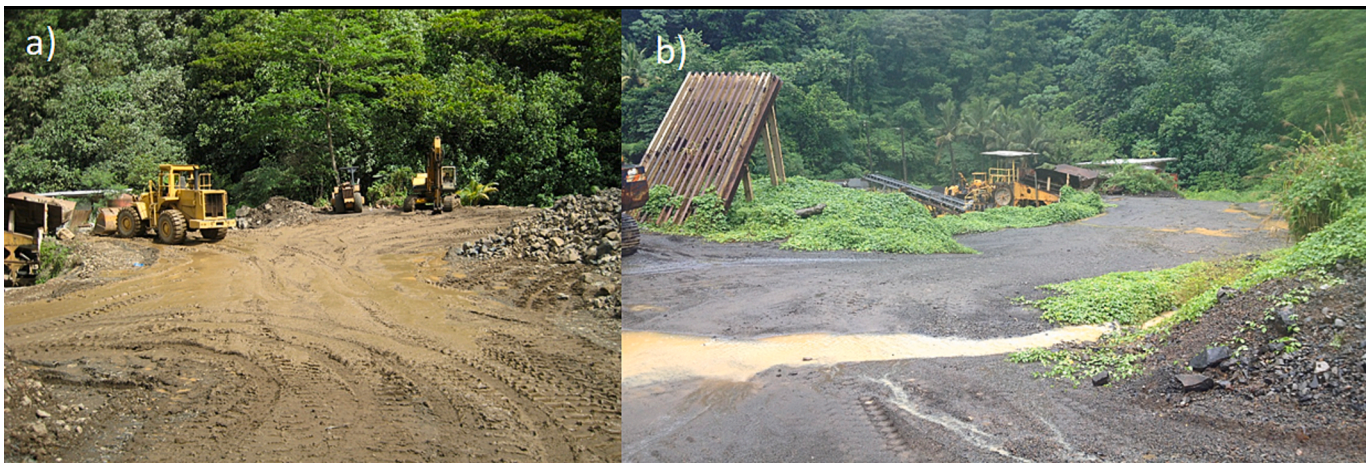

Fig. 3. Photographs of the upper processing platform a) before (2012) and b) after (2014) placement of gravel on unpaved surfaces and partial revegetation. Photo credit Alex Messina.

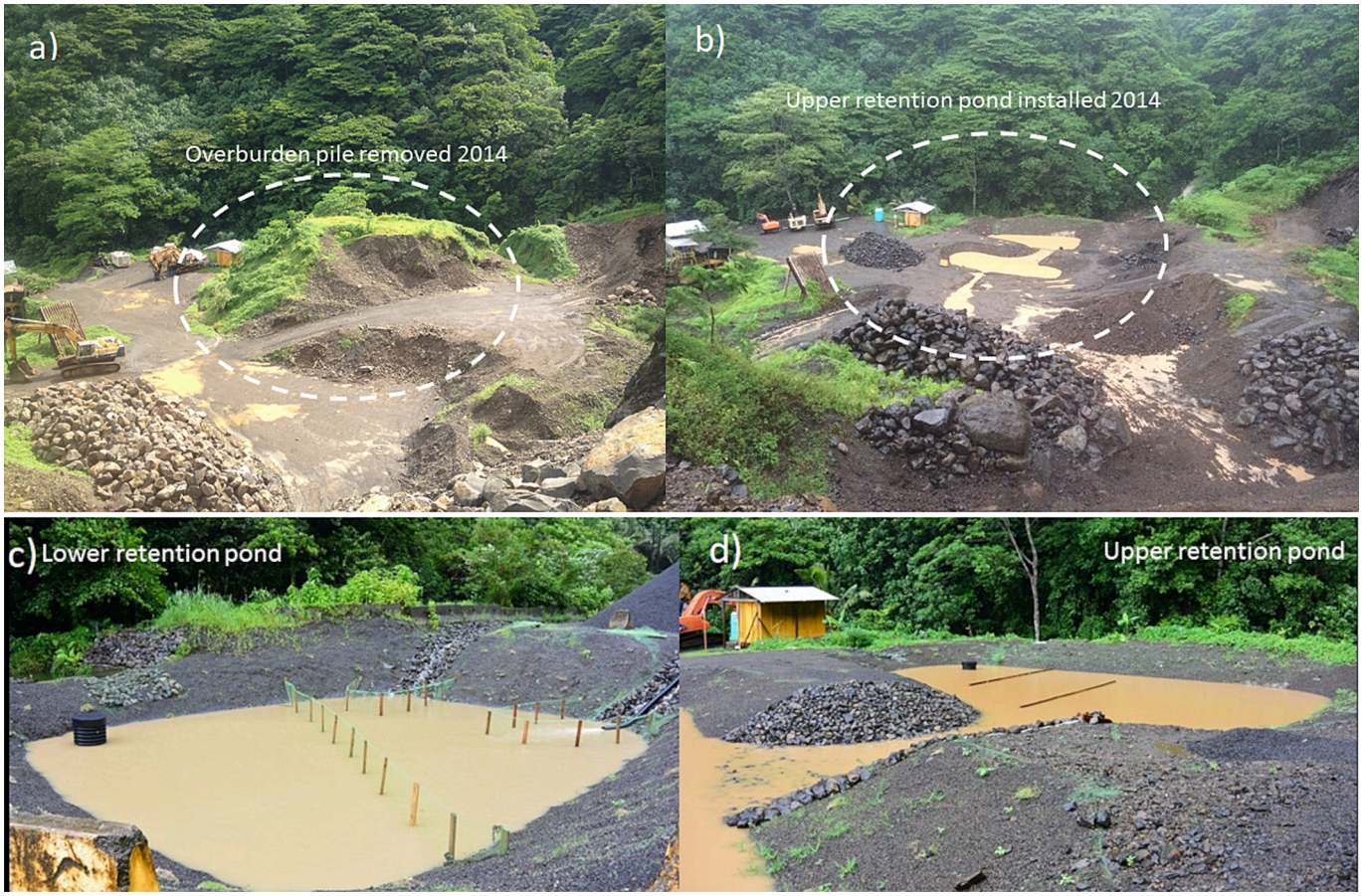

Fig. 4. The upper processing platform and excavation area a) before and b) after the installation of the upper retention ponds. c) Pond installed in the lower processing platform. c) Lower and d) upper retention ponds following a large rain storm. The retention ponds on the upper platform are connected by a gravel-lined spillway. Stand-pipes in the corner of each retention pond route water from the pond directly into the stream to prevent overflow. Photo Credit Alex Messina.

mitigation period only (RQ2, Section 3.3.1). Then, in order to quantify change over time while controlling for differences in storm size distribution among monitored periods, synthetic SSC, SSY and SSL values were estimated for each mitigation period using the Q_{max} values from a reference storm sequence (Feb-June 2016) and the SSY-Q_{max} or SSC-Q_{max} regression equations for each mitigation stage (Section 3.3.1). Uncertainty was quantified by varying the stormflow separation parameters and Monte Carlo sampling of the regression error (3.3.2). Each of these steps is described in more detail in each section below.

3.1. Discharge, turbidity and sediment monitoring

Stream water discharge ($m^3\ s^{-1}$), turbidity (NTU), and suspended sediment concentration (SSC mg L^{-1}) were measured during field campaigns spanning five years (2012–2016) (Fig. 5). One monitoring site (FOR) upstream of the quarry drains 0.9 km^2 of undisturbed forest. The

Table 1
Timeline of mitigation activities at the quarry.

August 2012	Groundwater seep drainage from upslope of the quarry diverted from quarry surface to stream
August 2012-February 2013	Gravel placed on unpaved roads, platform, and operational areas. Vegetation growth on stockpiles
October 22-November 4, 2014	Construction of retention ponds
November 2014	Installation of pond outlet structures
March 2015	Installation of final baffles in ponds

second site, downstream of the quarry (QRY), drains a total of 1.2 km^2, including all of the FOR watershed, the quarry (1.6 ha), and additional forest (Fig. 1). Details of the equipment and installations are described in Messina and Biggs (2016). Briefly, a recording tipping-bucket raingage was installed at the quarry in January 2012 (RG1 in Fig. 1), but rainfall data were not used for the load calculations. Non-vented pressure transducers and a barologger were installed at FOR in January 2012. The stage-discharge relationship at FOR was determined with a combination of area-velocity measurements and modeling with HEC-RAS (Messina, 2016; Messina and Biggs, 2016). The gauged site at FOR is a concrete flume that was stable and did not accumulate sediment throughout the monitoring period, so the stage-discharge relationship was invariant over time. Discharge downstream of the quarry was difficult to measure given channel conditions, and so was initially estimated as the product of the drainage area of the forest at QRY and the area-normalized discharge measured at FOR, plus the runoff from the quarry itself, calculated using observed rainfall during each storm and the Soil Conservation Service curve number approach (Dunne and Leopold, 1978) for dirt and gravel on fine-textured-soils. Discharge from

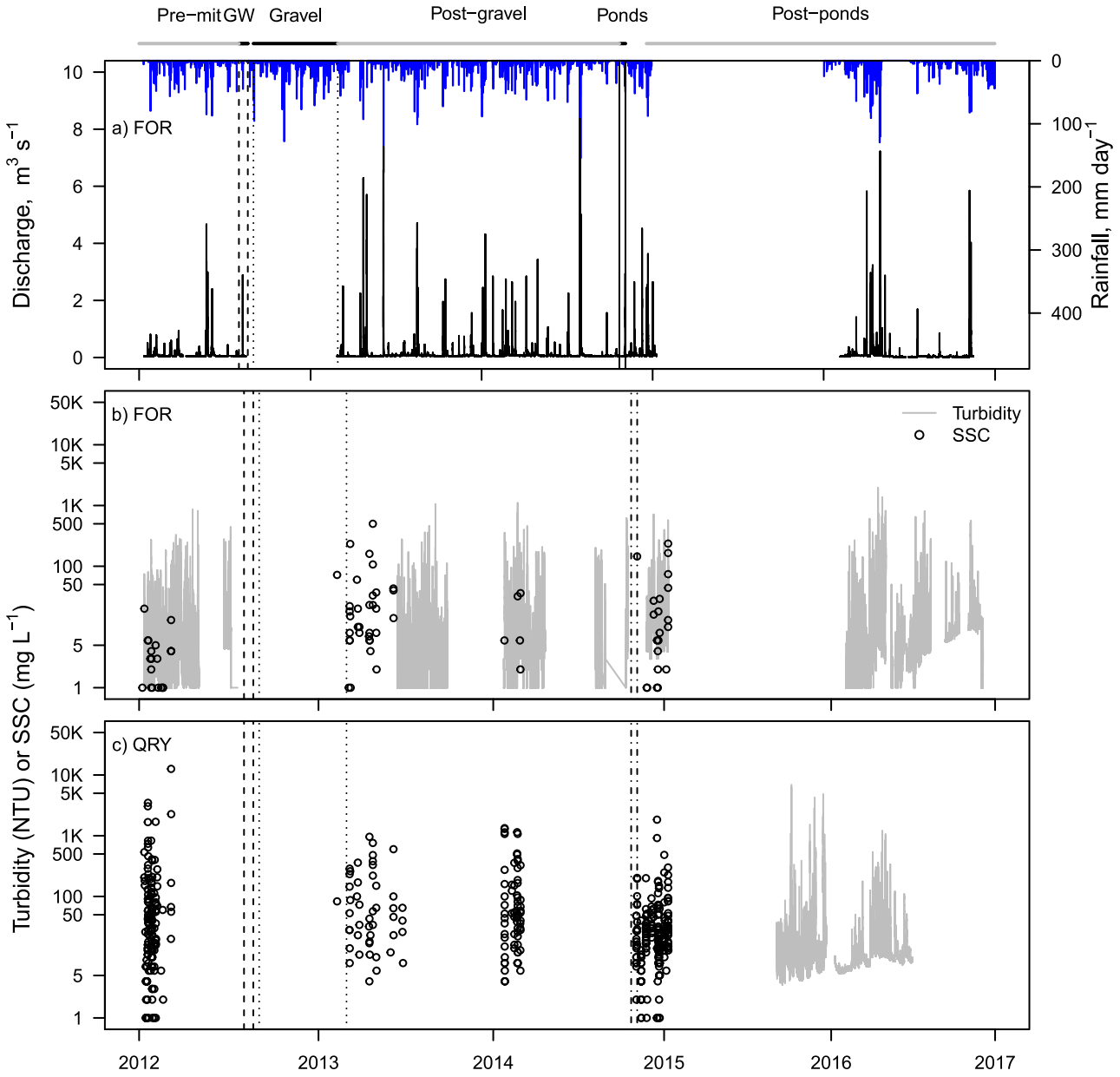

Fig. 5. Time series of data gathered during the study period including a) rainfall and stream water discharge at the forest site (FOR), and turbidity and suspended sediment concentration (SSC) at b) the forest (FOR) and c) downstream of the quarry (QRY). Bar at the top indicates the mitigation periods, including Pre-mitigation monitoring period (Pre-mit), diversion of groundwater seep (GW), emplacement of gravel ("Gravel"), Post-gravel monitoring period, installation of ponds Ponds) and Post-pond monitoring period (Post-ponds). Vertical lines indicate the start and end of the mitigation activities as labelled in the top bar, including GW (dashed lines), Gravel (dotted lines), and Ponds (dot-dash lines).

the quarry itself was a very small percentage of total flow during storms (1.6 ± 2.5 %), so for simplicity we estimated discharge at the quarry as the product of the area draining to the quarry (A_{QRY}) and the area-normalized discharge at FOR.

SSC was measured either directly using gravimetry on stream water samples, or indirectly using turbidity (T) and a turbidity-SSC relationship. Turbidimeters were installed and water samples collected at both FOR and QRY (Fig. 1). Timing of the deployment of the turbidimeters varied by location, and several different turbidimeters were used during the course of the field campaigns due to periodic failure, damage, theft, and changes in product availability. A Greenspan TS3000 turbidimeter was deployed at FOR from January 11, 2012 until its loss to theft in July 2012. A YSI 600 OMS was deployed at FOR in July 2012 and collected data March-September 2013, February 2014-April 2014, and October 2014-January 2015 (Fig. 5). In January 2016, additional turbidimeters (all Campbell Scientific OBS®) were installed at FOR and QRY and collected data through June 2016 (QRY) and Oct 2016 (FOR). The OBS were selected for all deployments after 2013 due to their superior correlations between turbidity and SSC (Messina, 2016). All turbidimeters were calibrated by the manufacturer prior to each deployment, and a calibration standard (1000 NTU) was tested on the tubidimeters at the end of each field deployment, with errors typically<5 % and always<15 % (Messina and Biggs, 2016). Water samples were collected for SSC analysis using both manual grab sampling at both locations, and an autosampler was installed at QRY in 2012. Water samples were analyzed for SSC using gravimetric methods (see Messina and Biggs, 2016). The stream water discharge, SSC and turbidity data are publicly available (Biggs and Messina, 2018).

Relationships between turbidity (T) and SSC were determined for each turbidimeter and location using linear regression (Messina and Biggs, 2016). The SSC-T relationship was robust with a high R^2 (0.82–0.93) and acceptable RMSE (46 mg/L) for the OBS (Messina and Biggs, 2016). Others have used a combination of discharge and turbidity to estimate SSC (Jastram et al., 2010; Ziegler et al., 2014) though turbidity alone is often used in either linear or power functions (Ram and Terry, 2016). We compared the use of linear and log-linear (power) functions for the SSC-T relationship, which yielded very similar RMSE values for the OBS; here we retain the use of linear SSC-T for the OBS as in Messina and Biggs (2016). Discharge was not a statistically significant additional predictor in the SSC-T regression, so turbidity alone was used to estimate SSC.

3.2. Storm identification and regression modeling

3.2.1. Storm identification for monitoring period

The discharge time series at FOR was separated into storm events using automated baseflow separation (EcoHydRology package v 0.4.12.1, Fuka et al., 2014) in R software (R Core Team, 2022). Baseflow separation in EcoHydRology is based on smoothing and separation rules developed by Lyne and Hollick (1979) and described in Nathan and McMahon (1990). Identification of storms depends on a filter parameter (f, range 0.90–0.99) and a minimum threshold value for stormflow (Q_{th}) that is required for a given discharge to be defined as stormflow. The values of f and Q_{th} impact the number of storms automatically detected using baseflow separation: low values of f and high values of Q_{th} separate compound events into separate events. Methods to quantify the impact of f and Q_{th} values on SSC, SSY and SSL estimates is described in section 3.3.2.

Storms where the ratio of maximum to minimum discharge was<1.5 were excluded from the analysis, as were storms with fewer than four SSC samples or turbidity values. Each storm hydrograph and the temporal distribution of SSC values during the storm were visually examined to ensure adequacy of sampling. Storms where samples were collected only at the very beginning and end of the storm were removed from the analysis. Total stormflow volume (V_{st}, m^3) was calculated as product of the mean discharge ($m^3\ s^{-1}$) and the duration of the storm (s), as determined by the storm separation algorithm.

3.2.2. Stormwise discharge and sediment metrics

SSC values, measured either directly in water samples or indirectly from the turbidity-SSC relationship, were linearly interpolated to the 15-minute resolution of the discharge data. The stormwise suspended sediment load (SSL, tons per storm) was then calculated as the sum of the products of discharge and SSC for each 15-minute period separately for each storm. Suspended sediment yield (SSY) was calculated as SSL divided by the drainage area at the sampling point (A_{FOR} or A_{QRY}). Stormwise mean SSC was calculated as SSL divided by V_{st}. Q_{max} was the maximum area-normalized discharge ($m^3\ s^{-1}\ km^{-2}$) observed during the part of the storm with SSC measurements. In most cases, sampling covered the whole storm, but for a few storms Q_{max} was different from the peak discharge from the whole storm because SSC sampling period did not include the peak discharge.

3.2.3. Regression models for SSC and SSL

We tested for correlations between event-wise SSY or event-mean SSC and Q_{max} (RQ1) using power functions, following Duvert et al (2012) and Messina and Biggs (2016):

$$SSY = \alpha_{SSY} Q_{max}^{\beta_{SSY}} \quad (1)$$

$$SSC = \alpha_{SSC} Q_{max}^{\beta_{SSC}} \quad (2)$$

where Q_{max} is the maximum area-normalized discharge observed during a storm ($m^3\ s^{-1}\ km^{-2}$), and α and β are parameters. α and β were estimated by log-transforming both sides, and adding an error term (ε):

$$\log(SSY or SSC) = \log(\alpha) + \beta \log(Q_{max}) + \varepsilon \quad (3)$$

Regression parameters were determined separately for pre-mitigation, post-gravel, and post-pond periods. In some cases, β changed with increasing Q_{max}, so piecewise regression was used as implemented in the *segmented* package (Muggeo, 2008) in R. We model SSY and not SSL as a function of Q_{max} in order to compare the SSY values and regression parameters for each sampling location (up and downstream of the quarry), controlling for watershed area. This follows Duvert et al. (2012), who used area-normalized values (SSY and Q_{max}) to compare rivers with different drainage areas.

The impact of the duration between storm events on SSY and SSC, which can be important in some settings (Mukundan et al., 2013) was tested by performing the regressions without and with inter-storm time (t_s) as an independent variable. t_s was calculated as the time between the beginning of a given storm and the end of the previous storm as defined by the hydrograph separation.

3.3. Mitigation impact and uncertainty analysis

3.3.1. Mitigation impact

Comparison of SSC, SSY and SSL for different time periods is complicated by differences in storm size distribution and data availability. Mitigation effectiveness was therefore quantified in two ways: 1) Turbidity, SSC, SSY and SSL were compared up and downstream of the quarry during baseflow and stormflow at FOR and QRY, post-mitigation period only; 2) Synthetic SSL values were estimated for each mitigation condition using a reference storm sequence:

$$SSL_{r,m} = \sum_{i=1}^{n} A_Q \alpha_{SSY,m} Q_{max,i}^{\beta_{SSY,m}} \quad (4)$$

where $SSL_{r,m}$ is the total SSL (tons) for the reference storm sequence in mitigation condition m (pre, post-gravel and post-ponds), i is an index of the storm number in the reference storm sequence, n is the number of storms in the reference storm sequence, A_Q is the drainage area at QRY (km^2), and $\alpha_{SSY,m}$ and $\beta_{SSY,m}$ are the regression parameters for the SSY-

Q_{max} regression (Eq. (1)) for mitigation condition m. The Q_{max} series of the reference storm sequence is the same for all mitigation conditions. The method varies only the regression parameters of the Q_{max}-SSY relationship by mitigation condition, keeping the distribution of Q_{max} constant.

The period of the reference storm sequence (February-June 2016, the post-ponds period) had continuous and complete discharge record with concurrent turbidity measurements (Fig. 2). This period covered the full range of Q_{max} values recorded in the other two mitigation stages. $SSL_{r,m}$ was calculated for all storms, and again for small storms only ($Q_{max} < 1$ m^3/s).Eq. (4) may result in changes in SSL if the relationship between Q_{max} and storm total volumetric discharge (V_{st}) changes between the reference storm sequence and a given mitigation period, even if SSC remains the same for a given Q_{max}. We therefore also calculated $SSL_{r,m}$ as:

$$SSL_{r,m} = \sum_{i=1}^{n} V_{st,i}\alpha_{SSC,m}Q_{max,i}^{\beta_{SSC,m}} \quad (5)$$

where $\alpha_{SSC,m}$ and $\beta_{SSC,m}$ are the regression parameters for the SSC-Q_{max} regression (Eq. (2)) for mitigation condition m, and $V_{st,i}$ is storm total discharge taken from the reference storm sequence. SSL_r estimated from these two methods will be identical if the relationships between Q_{max} and V_{st} are the same for all monitored periods, but different if the Q_{max}-V_{st} relationships differ among periods. In order to control for potential changes in Q_{max}-V_{st} relationships, we focus our analysis on SSL_r estimated using Eq. (5), and present results from Eq. (4) for comparison.

Bias correction (Duan, 1983; Crawford 1991), which accounts for the under-estimation of a dependent variable when using log-transformed variables in linear regression, was applied to all estimates of SSY and SSC. All SSL calculations assume that loading during baseflow conditions is minimal compared with loading during storms, which is supported by low SSC (<10 mg/L) and turbidity (<20 NTU) observed between storms (Section 4.2.2).

3.3.2. Uncertainty analysis

Several sources of uncertainty complicate calculations of SSC, SSY, and SSL (Harmel et al., 2006). Here we focus on the parameters and error in the SSY-Q_{max} relationships (Eq. (2)) and their impact on SSL_r. Other analyses (e.g. Harmel et al., 2006) include uncertainty in stage-discharge and SSC-T relationships, but are designed to estimate uncertainty in loads at a given location, while our goal is to assess uncertainty in the change in load due to mitigation activities. In Faga'alu, uncertainty in the SSC-T relationship was only present in the post-mitigation period, as all SSC values in the pre-mitigation period at QRY were from grab samples. Uncertainty in the SSY-Q_{max} and SSC-Q_{max} relationships is therefore the most important for our analysis.

The SSY-Q_{max} and SSC-Q_{max} regression parameters (α and β) changed with different flow separation parameters (f and Q_{th}) due in part to changes in the number of storms that result when using different separation parameters (Table S1, Table S2; Figs. S2–S8). We therefore quantified α, β, and SSL_r using several values of f (0.90, 0.95 and 0.99), and Q_{th} (0.01, 0.02, 0.03, 0.04, 0.08 m^3/s), where the plausible range in Q_{th} was determined by visual inspection of storm hydrographs. This resulted in fifteen f-Q_{th} parameter pairs, eight of which identified at least five storms with turbidity and/or SSC data in the pre-mitigation period. SSC estimates for large storms were unreasonably high for two f-Q_{th} pairs in the pre-mitigation stage due to high values of β (Table S2, Figs S6, S8); we therefore calculated SSL_r after excluding those two f-Q_{th} parameter pairs, for a total of six f-Q_{th} parameter pairs.

Uncertainty in SSL_r for each f-Q_{th} pair was quantified using Monte Carlo sampling of the error distribution of the SSY-Q_{max} or SSC-Q_{max} regressions, which was assumed to be a normal distribution with a mean of zero and standard deviation equal to the regression error (ε in Eq. (3)). The error distribution was sampled 1000 times for every storm for each f-Q_{th} pair and mitigation stage. The sampled random errors were added to log(SSY) or log(SSC) in Eq. (3), which were then inverse log-transformed into 1000 values of SSY, SSL_r, and change in SSL_r from pre-mitigation conditions for each f-Q_{th} pair and mitigation stage. The mean and standard deviation in SSL_r and change in SSL_r from SSL_r in pre-mitigation conditions were calculated for each f-Q_{th} pair and also for all six flow f-Q_{th} pairs combined (N = 6000 values, 1000 for each f-Q_{th} pair).

3.3.3. Statistical analysis

The relationship between Q_{max} and SSY or SSC (RQ1) was quantified using regression equations (3.2.3) and visualized by plotting Q_{max} against SSY or SSC for each mitigation stage; the p-value of the regression parameter β determined the significance of the SSY-Q_{max} and SSC-Q_{max} relationships at each mitigation stage. The statistical significance of differences in turbidity and SSL up and downstream of the quarry post-mitigation (RQ2) was determined with a t-test and box-plots of turbidity values, with separate tests and plots for baseflow (non-storm periods) and stormflow. The statistical significance of differences in SSL and SSC up and downstream of the quarry (RQ 2) and of changes in SSL_r and SSC_r during each mitigation stage (RQ3) were determined using t-tests.

4. Results

4.1. Storm characteristics

The baseflow separation algorithm identified between 44 and 61 storms with sufficient SSC data to calculate SSL, depending on the flow separation parameters (Table S1). The reference storm sequence, taken from the post-ponds period (February 15-June 16, 2016) had a total of 30–45 storms depending on the f-Q_{th} pair (Table S1). The pre-mitigation and post-gravel periods had fewer storms with SSC data (N = 5–9 each; Table S1) than the post-ponds period. Daily rainfall during the sampled period (Fig. 5) was below 100 mm for all but one storm (120 mm in February 2016), indicating that the sampled period did not include a large cyclone, where rainfall can reach 300–500 mm in a single day (Kostaschuk et al., 2003). A hurricane storm track database also suggests that no hurricanes passed over Tutuila during the monitored period (National Oceanic and Atmospheric Administration, 2023). Larger storms might be anticipated to occur in the watershed, especially given climate change (Marra and Kruk, 2017), with corresponding large sediment loads (Kostaschuk et al., 2003).

4.2. Sediment concentrations, yields, and loads

4.2.1. RQ1: How does storm size impact SSC and SSY in different mitigation stages?

Stormwise-mean SSC increased with increasing Q_{max} during all time periods at FOR and after mitigation at QRY (p-value of all $\beta < 10^{-5}$; Fig. 6; Table S2). β values were statistically insignificant ($p > 0.05$) for SSY in the pre-mitigation period and for SSC in both pre-mitigation and post-gravel periods (Table S2). Stormwise mean SSC at FOR was nearly 100x higher during the largest storms compared with the smallest storms, highlighting the importance of controlling for storm size when documenting the effectiveness of mitigation. Pre-mitigation, SSC at QRY was highest for very small storms ($\beta < 0$) for some f-Q_{th} pairs (Table S2; Figs. 6; S2; S5; S7); other f-Q_{th} pairs did not separate out small storms and had a positive β for SSC (Figs. S3, S4, S6, S8).

4.2.2. RQ2: How do turbidity, SSC, SSY, and SSL compare upstream and downstream of the quarry following mitigation, during baseflow and stormflow, for a range of storm sizes?

In the final post-mitigation period (post-ponds), turbidity was the same above and below the quarry during stormflow ($p > 0.1$), and slightly but statistically significantly higher ($p = 0.05$) downstream of the quarry (QRY) during baseflow (Fig. 7). The higher turbidity at QRY during baseflow is consistent with field observations that the retention

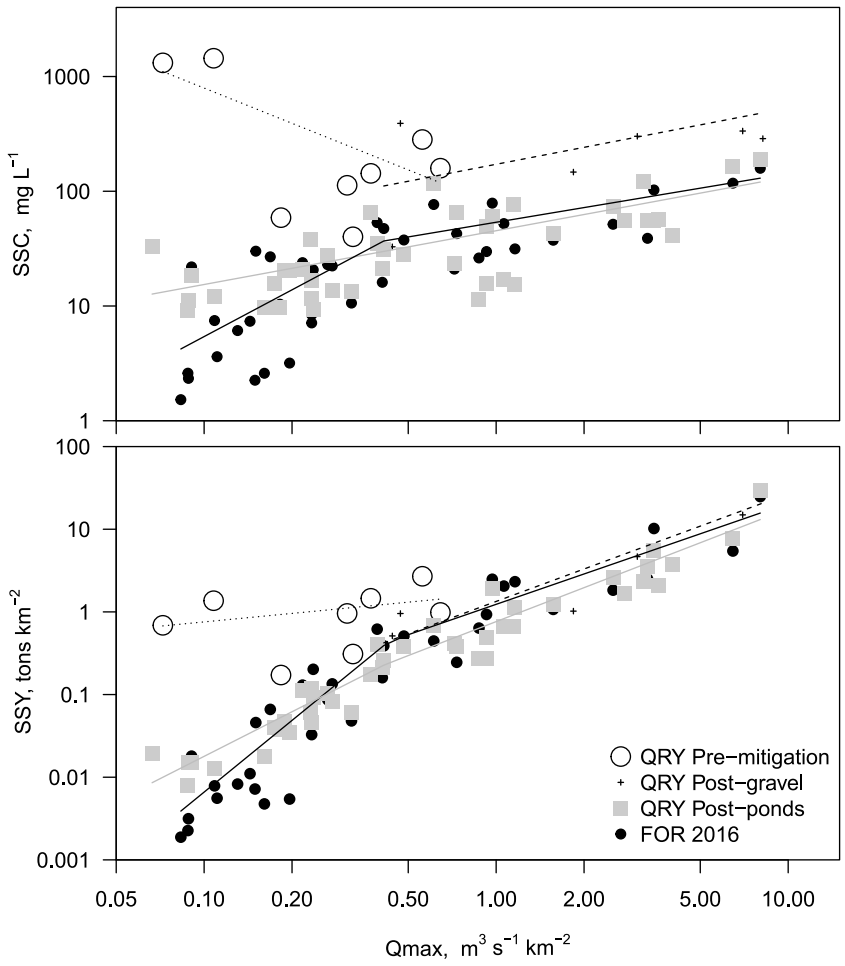

Fig. 6. A)Suspended sediment concentration (SSC) and b) load (SSL) versus Q_{max} for each storm event at the forest (FOR) and quarry (QRY), by mitigation period. Stormflow separation performed using filter parameter (f) of 0.90 and minimum stormflow threshold (Q_{th}) of 0.02.

ponds slowly release turbid water to the stream under baseflow conditions.

SSL_r and SSC_r were slightly different between QRY and FOR in the post-mitigation period: SSL was 68 tons at QRY versus 76 tons at FOR for all storms, and 5.0 tons at both locations for small storms (Table 2; Fig. 6). We conclude that SSL_r and SSC_r downstream of the quarry were statistically similar to SSL_r and SSC_r from the forest in the post-ponds period, which includes the impact of both gravel and ponds.

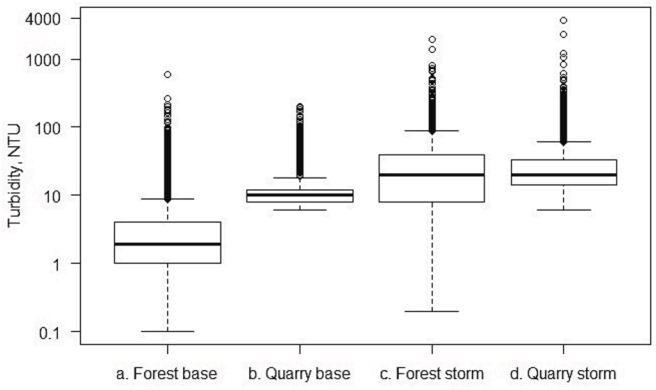

Fig. 7. Boxplot of turbidity at the forest (FOR) and quarry (QRY) locations during baseflow and stormflow, post-pond conditions.

Table 2
Suspended sediment load (SSL_r, tons) and concentration (SSC_r, mg/L) for the reference storm sequence downstream of the quarry (QRY), at the forest (FOR) and percent reduction in SSL_r at QRY compared to pre-mitigation conditions. SSL_r and SSC_r were calculated for all storms Feb-June 2016 using six combinations of separation factors (Table S1). SSL and SSC at QRY were estimated using SSC-Q_{max} regressions for each mitigation stage (Eq. (5)), with Monte Carlo sampling of the regression error (ε).

Mitigation stage	SSL_r	SSC_r	Change in SSL_r	
	tons	mg/L	tons	%
All storms				
QRY Pre-mitigation	474 ± 234	472 ± 253	–	–
QRY Post-gravel	279 ± 97	270 ± 86	−195 ± 250	−31 ± 26
QRY Post-pond	68 ± 15	67 ± 14	−406 ± 236	−82 ± 9
FOR Forest	76 ± 34	73 ± 30	–	–
Small storms				
QRY Pre-mitigation	64 ± 16	456 ± 111	–	–
QRY Post-gravel	23 ± 6	161 ± 43	−41 ± 15	−63 ± 11
QRY Post-pond	5 ± 1	35 ± 8	−59 ± 16	−92 ± 3
FOR Forest	5 ± 1	34 ± 10	–	–

4.2.3. RQ3: Did mitigation activities reduce SSC and SSL downstream of the quarry over time, controlling for differences in the storm size distribution among monitored periods?

SSL_r and SSC_r at QRY were lower following mitigation, with the largest changes for small storms (Fig. 6). The mean SSL_r for all *f*-Q_{th} pairs together (N = 6000 Monte Carlo samples) using Eq. (5), was 82 ± 9 % lower post-mitigation for all storms and 92 ± 3 % lower for small storms in the reference sequence (Table 2). SSL_r and its percent reduction varied significantly by *f*-Q_{th} pair (Table S3, S5): mean pre-mitigation SSL_r from Eq. (5) ranged from 326 to 817 tons and the percent reduction from pre-mitigation conditions to post-ponds ranged from 76 % to 91 % depending on the *f*-Q_{th} pair (Table S5). The large range in pre-mitigation SSL_r was due to large error in the SSY-Q_{max} regression for a given *f*-Q_{th} pair caused by the small number of storms sampled pre-mitigation (N = 5–8), and to differences in the number of storms among *f*-Q_{th} pairs (Table S1).

The estimated reduction in SSL_r from pre- to post-mitigation conditions (post-ponds) depended on which equation was used to calculate SSL_r (Eqs. (4) or (5); Table 2 and Table S4). Stormflow volumes (V_{st}) were smaller for a given Q_{max} in the pre-mitigation and post-gravel periods compared with the reference storms sequence, with the largest difference in the post-gravel period (Fig. S9). SSL_r was therefore higher in both the pre-mitigation condition (+41 %) and post-gravel condition (+115 %) when using the SSC-Q_{max} regression (Eq. (5)) than when using the SSY-Q_{max} regression (Eq. (4)), because V_{st} from the reference storm sequence used in Eq. (5) was larger than V_{st} from the monitored period used in Eq. (4) for a given Q_{max} (Tables S4 and S5). The storm metrics are calculated from discharge measured at the forest site (FOR), so the changes in the Q_{max}-V_{st} relationship among monitored periods is due to natural variability and not to management at the quarry: storms in the reference sequence had higher baseflow and longer recession limbs than storms in the post-gravel period. Percent reductions in SSL_r post-mitigation were therefore larger when using SSC-Q_{max} regressions (Eq. (5), 82 ± 9 %) than when using SSY-Q_{max} regressions (Eq. (4), Table S4, 63 ± 20 %). The relative importance of gravel and ponds also depended on the regression used: the SSC-Q_{max} regressions (Eq. (5)) estimated a smaller percent reduction in SSL_r during the post-gravel condition (31 %) than the SSL-Q_{max} regression (Eq. (4)) (48 %), while the percent reduction in SSL_r post-ponds was larger when using Eq. (5) (82 %) than when using Eq. (4) (63 %). Ponds were more important than gravel when using SSC-Q_{max} regressions, while gravel was more important than ponds when using SSY-Q_{max} regressions for all storms. Both regressions suggest that gravel was more important than ponds for small storms, but this conclusion depends on a small number of small storms sampled during the post-gravel period.

The total load reduction during the reference storm sequence was 250 tons (50 tons $month^{-1}$, Eq. (4), Table S4) or 406 tons (81 tons $month^{-1}$, Eq. (5), Table 2). Assuming that all of the excess load during the pre-mitigation condition was from the quarry surface (1.6 ha), this is equivalent to 37,500 to 60.750 tons km^{-2} y^{-1}. Ponds alone reduced SSL_r by 43 tons, or 8.6 tons $month^{-1}$ when using SSY-Q_{max} regressions (Eq. (4)), and 211 tons, or 42.4 tons $month^{-1}$ when using SSC-Q_{max} regressions (Eq. (5)). Given the total capacity of the traps (1450 tons) and assuming constant mean monthly loading rates, this suggests the traps could fill approximately every 14 years (estimated using Eq. (4)) or 2.8 years (estimated using Eq. (5)), but more frequent maintenance would be required to sustain a high trap efficiency.

5. Discussion

We document that 1) storm size has a large but predictable impact on SSC and SSL both upstream and downstream of the mitigation site (quarry); 2) following sediment mitigation, SSL downstream of the mitigation site was similar to or less than the SSL upstream of the mitigation site; 3) mitigation reduced SSL over time downstream of the mitigation site, controlling for storm size distribution, and reduced SSL the most for small storms; and 4) gravel placement was an important component of mitigation, but quantification of its impact was complicated by differences in sampled storm characteristics among monitored periods. We discuss each of these points below.

5.1. Storm size and sediment loads

Maximum stormwise area-normalized discharge (Q_{max}) correlated strongly with SSC and SSY: stormwise mean SSC from the forest was up to 100x higher during large storms compared with small storms, highlighting the importance of accounting for storm size when documenting the impact of mitigation on stream SSC and SSL. Large storms are rare and sometimes dangerous to sample, so the impacts of mitigation will always be more uncertain for large storms compared with small storms (Kostaschuk et al., 2003). Others have also found that Q_{max} is a strong predictor of suspended sediment concentrations and loads (Duvert et al, 2012; Rankl, 2004). The slopes of the SSY-Q_{max} relationship (β) downstream of the quarry (QRY, Table S2, not piecewise) ranged from 1.42 to 1.53 in the post-mitigation period, which is similar to the ranges from other studies compiled by Duvert et al (2012) (range 1.07–1.72, outliers at 2.29 and 2.45). Values of β greater than one indicate that SSY increases non-linearly with increasing Q_{max}, which results in disproportionate contribution of large storms to sediment loads. At the Faga'alu forested watershed (FOR), β decreases with increasing Q_{max}, marked by an inflection in the piece-wise linear regression around Q_{max} of 0.4 m^3 s^{-1} km^{-2}. While Duvert et al (2012) did not model such an inflection point, some of their SSY data (e.g. Fig. 5 in Duvert et al. 2012) show very low SSY for low Q_{max} (<0.1 $m^3 s^{-1}$ km^{-2}) and SSY is often overpredicted by a linear model for low Q_{max}, suggesting that their and other watersheds may also show non-linear or piecewise linear SSY-Q_{max} relationships.

The slope of the relationship between Q_{max} and SSC (β_{SSC}) was positive for the forest (FOR) and quarry (QRY) site after pond installation, but was slightly negative at QRY in the pre-mitigation period for some storm separation values (Table S2). Flat or negative SSC-Q relationships indicate highly erodible surface sediments of a relatively fixed quantity that can be transported for a wide range of discharges (Asselman, 2000). This is consistent with an active quarry, where new and highly erodible fine sediment is continuously generated between storms by processing activities. The negative SSC-Q_{max} relationship observed downstream of the quarry in pre-mitigation conditions suggests that sediment eroded from the quarry even during small events, and that discharge from the forest diluted SSC from the quarry at higher flows. The impact of mitigation on SSC decreased with increasing Q_{max} due to higher SSC from the forested parts of the watershed during large storms.

Our sampling period included mostly small to medium-sized storms (<120 mm of rainfall per day), while much larger storms have been observed throughout the Pacific during tropical cyclones. Extreme events are anticipated to have correspondingly higher SSC and SSL (Kostaschuk et al., 2003), and may dominate the long-term (decadal) SSL. Cyclones can also damage coral reefs, and may be a critical process driving long-term sediment loads and coral reef structure. The role of large events in sediment loading to the coast in American Samoa and elsewhere in the Pacific requires further research.

Our estimated mean SSC at the undisturbed site (FOR, 86 mg L^{-1}) was similar to SSC observed in Hawai'i (Hanalei, 63 mg L^{-1}) (Ferrier et al., 2013; Stock and Tribble, 2010), which has similar rainfall (3866 mg L^{-1}) to Faga'alu (3,247 mm y^{-1}), suggesting that SSC from Faga'alu is representative of other Pacific islands on volcanic terrain. Other studies have also found that disturbance of a small fraction of a watershed area can increase SSC or SSY several fold (Stock et al., 2010). SSC at Faga'alu quarry (QRY) was 6.5 times SSC at the forest (FOR), which is similar to increases of 3–9 times in watersheds with unpaved roads in the US Virgin Islands (Ramos-Scharrón and MacDonald, 2005) and 5–10 times in areas with mines on Papua New Guinea (Hettler et al., 1997). The percent contribution of the quarry subwatershed to the pre-mitigation

sediment load at QRY (84 %) is larger than the percent contribution of the quarry subwatershed to the load at the ocean estimated by Messina and Biggs (2016) (~50 %), because the incremental watershed between QRY and the ocean contains additional sediment sources including agriculture and the village.

5.2. Quantification of mitigation effectiveness

The effectiveness of sediment mitigation was quantified using two main methods: comparison of SSC and SSL up and downstream of the mitigation site in the post-mitigation period only, and comparison of SSC and SSL downstream of the mitigation site over time, controlling for storm size by using a reference storm sequence to estimate SSC and SSL with different regression equations to predict SSY and SSC from Q_{max} for each mitigation period. The up-down comparison was the most straightforward, since the same storms were sampled at both locations, but the comparison does not determine how much SSL changed from pre-mitigation conditions or the impact of different phases of mitigation. The up-down comparison also assumes that the only reason for differences in SSL between up and downstream is human disturbance; natural variability in rock type, soil texture or topography could complicate the comparison among sites.

Quantification of load reduction over time using observed SSL at one location can quantify changes due to mitigation, but results depend on the size distribution of sampled storms and on the relationship between storm metrics, especially Q_{max} and stormflow volume (V_{st}). In our case study, the pre-mitigation period had no storms with Q_{max}>0.8 $m^3\ s^{-1}\ km^{-2}$, while the post-gravel period had large storms (Q_{max} up to 7–8 $m^3\ s^{-1}\ km^{-2}$), but few very small storms (Q_{max} 0.5 $m^3\ s^{-1}\ km^{-2}$) (Fig. 6). This therefore required extrapolation of the SSY-Q_{max} and SSC-Q_{max} relationships beyond the range of sampled storms in order to estimate SSL for the reference storm sequence. Extrapolation introduces errors, which we incorporate into our analysis by using SSY-Qmax regressions for different storm separation thresholds. Extrapolation was most important for large storms in the pre-mitigation period, and for small storms in the post-gravel period (Fig. 6). Comparison of SSL_r for small storms between the pre-mitigation and post-mitigation conditions did not require extrapolation, since both periods had good coverage of a range of small storm sizes. Despite the problems with extrapolation, we calculated SSL_r for the full range of observed storms in all three periods in order to quantify and highlight the potential importance of small and large storms for SSL and mitigation effectiveness. Our objective is to illustrate a method to calculate mitigation effectiveness that acknowledges and quantifies uncertainty introduced by both the range of storm sizes sampled, and by variability in sediment loads for a given storm size.

The relationship between storm metrics, especially maximum storm discharge (Q_{max}) and stormflow volume (V_{st}) had important impacts on estimated sediment reduction by mitigation stage. In our dataset, storms in in the post-gravel period had shorter time bases and lower V_{st} for a given Q_{max} than the reference storm sequence. This resulted in lower event-wise SSY values for the post-gravel sequence due only to changes in stormflow characteristics. Gravel had measurable impacts on SSL using all methods, but larger impacts when using SSY-Q_{max} regressions (Eq. (4)) due to changes in the Q_{max}-V_{st} relationship.

These issues highlight three main weaknesses of the method. First, the results can depend on the size distribution of sampled storms in each mitigation period. Sampling of storms with a range of sizes in all mitigation periods is required for robust estimation of mitigation effectiveness. This is particularly problematic for large storms, which are infrequent and difficult or dangerous to sample. This issue is common to all methods to estimate mitigation effectiveness by monitoring storms, and is most severe when comparing sediment loads for different periods directly without considering differences in storm size distribution. Our stormwise method attempts to reduce the impact of variations in the size distribution of storms among mitigation periods by calculating loads for a reference storm sequence, which controls for variations in the size distribution. Robust results still require field data for a range of storm sizes to accurately parameterize the SSY-Q_{max} and SSC-Q_{max} regression equations; failure to sample a range of storms requires extrapolation beyond the range of sampled storms and introduces additional uncertainty. Second, the results can be impacted by changes in storm characteristics between monitored periods, especially the relationship between Q_{max} and V_{st}. This effect is largest when using SSY-Q_{max} regressions to estimate SSL for a storm reference sequence, so sensitivity analysis needs to be conducted to determine the impact of changes in these two storm metrics by also estimating SSL_r from the SSC-Q_{max} regressions. Finally, variations in rainfall intensity and sequence can impact the effectiveness of mitigation activities, introducing additional variation and error in estimated effectiveness. The standard deviation of SSL_r for each mitigation stage was 20–50% of the mean, pointing to the large uncertainty due to storm characteristics or sediment availability that were not monitored here. Additional work could quantify the main reasons for the high inter-storm variability and introduce additional predictor variables.

5.3. Recommendations for quantifying mitigation effectiveness

Stormwise metrics have advantages in assessing SSL and mitigation effectiveness, including: 1) removal of intra-storm hysteresis in SSC-Q relationships 2) simplification of the analysis by summarizing each storm by a single metric and 3) leveraging relationships between storm metrics (here, Q_{max}) and SSL (see also Duvert et al., 2012) to estimate SSL for storms that were not sampled for sediment. The disadvantage of stormwise metrics is the need to sample over the whole hydrograph in order to have accurate estimates of SSL, while sediment rating curves based on individual SSC-Q pairs can use data from storms with partial sampling coverage or individual grab samples. We took individual samples throughout storm events; volume-weighted composite sampling is recommended to reduce cost and laboratory analysis time. Regardless of the method used, sampling over a range of storm sizes and determining the relationship between storm size and load is essential for quantifying mitigation effectiveness.

5.4. Implications for mitigation

Mitigation reduced turbidity and sediment concentrations and loads downstream of the quarry back to near or below the natural background during storms. The mitigation was applied to a small (<1%) percentage of the watershed, using relatively simple techniques of gravel placement and pond construction. Gravel placement had a larger impact on SSL than pond installation for small storms, though the order of activity may impact this conclusion; ponds may have had a smaller impact because gravel placement had already reduced loads. Gravel placement has the advantage of increasing the safety and operability of the quarry and so is more likely to be maintained over time, while ponds, while effective, require regular maintenance to retain sediment effectively. Overall, we found that mitigation of a small fraction of a watershed's area effectively reduced sediment load to near the natural background.

Our observations are consistent with other studies, where a relatively small fraction of a watershed area often contributes most of the sediment load (Stock et al, 2010). Patches of bare soil that are recently cleared or repeatedly mechanically disturbed, such as on construction sites, tilled agricultural fields, or our actively managed quarry, often produce the largest sediment loads, up to 100 s of times the pre-disturbance background (Wolman, 1967). Assuming that all of the excess load during the pre-mitigation condition was from the quarry surface, we estimate that quarry under pre-mitigation conditions produced 37,500 to 60.750 tons $km^{-2}\ y^{-1}$, with a lower-bound estimate of 13,200 tons $km^{-2}\ y^{-1}$ (Table S3, f 0.95 Q_{th} 0.03). This compares well with other observations of sediment yield from construction sites, of up to 55,000 tons $km^2\ y^{-1}$ for a site with much lower rainfall of 1100 mm y^{-1} (Wolman, 1967).

In forested areas, unpaved surfaces such as logging roads can produce a majority of the sediment at the watershed scale (Reid and Dunne, 1984). Others have also found that mitigation can be effective, including settling ponds (Mountjoy et al, 2005), which can retain ~ 80 % of incoming sediment (Gharabaghi et al., 2006), which is comparable to the reduction in SSL that we observed post-mitigation (both gravel and ponds). Road stabilization by paving is also very effective: paved roads yield only 1 % as much sediment as unpaved roads in the Pacific Northwest (Reid and Dunne, 1984). Best-management practices may be insufficient to protect stream ecosystems where land disturbance is widespread (Hogan et al, 2014). The quarry in Faga'alu was the only disturbance in the monitored portion of the watershed and was relatively small, resulting in successful mitigation that was detectable at the watershed scale.

6. Conclusion

Stormwise monitoring of discharge and suspended sediment concentration (SSC) demonstrated that 1) SSC and loads (SSL) increased markedly with increasing storm size, suggesting that storm size distribution is important to control for when quantifying mitigation effectiveness; 2) stormwise metrics (Q_{max}) were good predictors of SSC and load (SSL), allowing quantification of mitigation effectiveness, controlling for storm size and 3) mitigation of a small fraction of the watershed reduced sediment concentrations and loads to forested background levels. The post-mitigation SSC and SSL were similar both upstream and downstream of the mitigation site (quarry), suggesting that the site had been restored to its pre-disturbance load. While the long-term impact of mitigation on SSL has not been measured, gravel placement, which also assists quarry operation, was effective in reducing loads, suggesting that the ongoing maintenance of roads and platforms should continue.

Few studies have quantified the efficacy of mitigation activities implemented to reduce LBSP in watersheds draining to coral reefs. This novel approach can be replicated in other watersheds adjacent to coral reefs to measure reductions of LBSP into the receiving waters where coral is threatened by impacts from sedimentation. This information is important to coral reef managers so they can direct limited resources to activities known to be effective and improve water quality conditions and support more resilient coral reef ecosystems.

CRediT authorship contribution statement

T.W. Biggs: Conceptualization, Methodology, Software, Formal analysis, Writing – original draft, Visualization, Supervision, Project administration, Funding acquisition. **A.T. Messina:** Conceptualization, Methodology, Software, Formal analysis, Investigation, Writing – original draft, Visualization, Supervision, Project administration, Funding acquisition. **S.H. Rice:** Conceptualization, Writing – review & editing, Project administration, Funding acquisition. **M.C. Hattori:** Conceptualization, Writing – review & editing, Investigation, Supervision. **H. McMillan:** Conceptualization, Methodology, Writing – review & editing.

Declaration of Competing Interest

The authors declare that they have no known competing financial interests or personal relationships that could have appeared to influence the work reported in this paper.

Data availability

Data published in NCEI link provided in the reference list.

Acknowledgements

This project was funded by the National Oceanic and Atmospheric Administration (NOAA) Coral Reef Conservation Program (CRCP) opportunity numbers NOAA-NOS-OCRM-2011-2002594 (FY11) and NA-13-NOS-4820013 (FY13), by the National Fish and Wildlife Federation, Grants 0302.15.048808 (2015) and 0302.19.064874 (2019), and by San Diego State University Doctoral support for AM. The American Samoa Environmental Protection Agency (ASEPA) and Coral Reef Advisory Group (CRAG) provided ongoing logistical and field support, with special thanks to ASEPA personnel including Director Akemo Pato (2015); Deputy Director (2015) and current Director Faamao O. Asalele Jr; Victor Tuiasosopo; Christianera Tuitele; and field support from Siumu Fa'ai'uaso. Hideyo Hattori (NOAA) and Motu Vaeoso, Kim McGuire, Kristine Bucchianeri, and Sabrina Woofter from the Coral Reef Advisory Group (CRAG) provided logistical support.

Appendix A. Supplementary data

Supplementary data to this article can be found online at https://doi.org/10.1016/j.jhydrol.2023.130525.

References

Asselman, N.E.M., 2000. Fitting and interpretation of sediment rating curves. J. Hydrol. 234, 228–248. https://doi.org/10.1016/S0022-1694(00)00253-5.

Biggs, T.W., Messina, A., 2018. Stream discharge, turbidity, and suspended sediment concentration in Faga'alu watershed, American Samoa from 2012–01-12 to 2016–11-15. Nactional Centers for Environmental Information (NCEI). Accession 0191818.

Crawford, C.G., 1991. Estimation of suspended-sediment rating curves and mean suspended-sediment loads. J. Hydrol. 129, 331–348. https://doi.org/10.1016/0022-1694(91)90057-O.

Duan, N., 1983. Smearing Estimate: A Nonparametric Retransformation Method. J. Am. Stat. Assoc. 78, 605–610. https://doi.org/10.1080/01621459.1983.10478017.

Dunne, T., Leopold, L.B., 1978. Water in Environmental Planning. New York, W.H, Freeman and Company.

Duvert, C., Nord, G., Gratiot, N., Navratil, O., Nadal-Romero, E., Mathys, N., Némery, J., Regüés, D., García-Ruiz, J.M., Gallart, F., Esteves, M., 2012. Towards prediction of suspended sediment yield from peak discharge in small erodible mountainous catchments (0.45–22km2) of France. Mexico and Spain. J. Hydrol. 454–455, 42–55. https://doi.org/10.1016/j.jhydrol.2012.05.048.

Fabricius, K.E., 2005. Effects of terrestrial runoff on the ecology of corals and coral reefs: review and synthesis. Mar. Pollut. Bull. 50 (2), 125–146.

Ferrier, K.L., Perron, J.T., Mukhopadhyay, S., Rosener, M., Stock, J.D., Huppert, K.L., Slosberg, M., 2013. Covariation of climate and long-term erosion rates across a steep rainfall gradient on the Hawaiian island of Kaua'i. Geological Society of America Bulletin 125 (7-8), 1146–1163.

Fuka, D., Walter, M., Archibald, J., Steenhuis, T., Easton, Z., 2014. EcoHydRology: A community modeling foundation for Eco-Hydrology.

Gharabaghi, B., Fata, A., Van Seters, T., Rudra, R.P., MacMillan, G., Smith, D., Li, J.Y., Bradford, A., Tesa, G., 2006. Evaluation of Sediment Control Pond Performance at Construction Sites in the Greater Toronto Area. Canadian Journal of Civil Engineering 33, 1335–1344. https://doi.org/10.1139/l06-074.

Harmel, R.D., Cooper, R.J., Slade, R.M., Haney, R.L., Arnold, J.G., 2006. Cumulative uncertainty in measured streamflow and water quality data for small watersheds. Trans. ASABE 49, 689–701. https://doi.org/10.13031/2013.20488.

Hettler, J., Irion, G., Lehmann, B., 1997. Environmental Impact of Mining Waste Disposal on a Tropical Lowland River System: A Case Study on the Ok Tedi Mine. Papua New Guinea. *Mineralium Deposita* 32 (3), 280–291.

Hogan, D.M., Jarnagin, S.T., Loperfido, J.V., Van Ness, K., 2014. Mitigating the Effects of Landscape Development on Streams in Urbanizing Watersheds. J American Water Resour Assoc 50 (1), 163–178.

Holst-Rice, S., Messina, A.T., Biggs, T.W., Vargas-Angel, B., Whitall, D., 2016. Baseline Assessment of Faga'alu Watershed: A Ridge to Reef Assessment in Support of Sediment Reduction Activities and Future Evaluation of their Success. Silver Spring, MD. https://doi.org/10.7289/V5BK19C3.

Horsley Witten Group, 2014. Basis of Design Memo for Samoa Maritime Erosion and Sediment Control Corrective Action Plan. Sandwich, MA.

Inman, D.L., Jenkins, S.A., 1999. Climate Change and the Episodicity of Sediment Flux of Small California Rivers. J. Geol. 107, 251–270. https://doi.org/10.1086/314346.

Jastram, J.D., Zipper, C.E., Zelazny, L.W., Hyer, K.E., 2010. Increasing precision of turbidity-based suspended sediment concentration and load estimates. J. Environ. Qual. 39 (4), 1306–1316.

Kondolf, G.M., 1998. Lessons learned from river restoration projects in California. Aquat. Conserv. Mar. Freshw. Ecosyst. 8, 39–52. https://doi.org/10.1002/(SICI)1099-0755(199801/02)8:1<39::AID-AQC250>3.0.CO;2-9.

Kostaschuk, R., Terry, J., Raj, R., 2003. Suspended sediment transport during tropical-cyclone floods in Fiji. Hydrol. Process. 17, 1149–1164. https://doi.org/10.1002/hyp.1186.

Lyne, V., Hollick, M., 1979. Stochastic time-variable rainfall-runoff modelling. In: Institute of Engineers Australia National Conference. Institute of Engineers Australia Barton, Australia, pp. 89–93.

Mainstone, C.P., Dils, R.M., Withers, P.J.A., 2008. Controlling sediment and phosphorus transfer to receiving waters – A strategic management perspective for England and Wales. J. Hydrol. 350, 131–143. https://doi.org/10.1016/j.jhydrol.2007.10.035.

Horsley Witten Group Inc., 2013. Faga'alu Watershed Plan Implementation Supplement. Sandwich, MA. https://www.ncei.noaa.gov/data/oceans/coris/library/NOAA/CRCP/project/20767_Leau/130322_Fagaalu_Watershed_Implementation_Supplement_final.pdf, access date Nov 20, 2023.

Marra, J.J., and M.C. Kruk. "State of Environmntal Conditions in Hawaii and the U.S Affiliated Pacific Islands under a Changing Climate: 2017." NOAA National Centers for Environmental Information (NCEI), 2017.

McDougall, I., 1987. Age and Evolution Oi the Volcanoes of Tutuila, American Samoa. Pacific Science 39 (4), 311–320.

Messina, A., 2016. Terrigenous sediment dynamics in a small, tropical, fringing-reef embayment (PhD Dissertation). Department of Geography, San Diego State University, San Diego, CA.

Messina, A.M., Biggs, T.W., 2016. Contributions of human activities to suspended sediment yield during storm events from a small, steep, tropical watershed. J. Hydrol. 538, 726–742. https://doi.org/10.1016/j.jhydrol.2016.03.053.

Milliman, J.D., Meade, R.H.., 1983. World-Wide Delivery of River Sediment to the Oceans. J. Geol. 93, 1–21.

Morehead, M.D., Syvitski, J.P., Hutton, E.W.H., Peckham, S.D., 2003. Modeling the temporal variability in the flux of sediment from ungauged river basins. supply flux sediment along Hydrol. pathways Anthropog. Influ. Glob. scale 39, 95–110. https://doi.org/10.1016/S0921-8181(03)00019-5.

Mountjoy, K.J., Diggon, H.M., Vickery, B.J., 2005. Performance of Sediment Control Settling Ponds. Texada Quarry, British Columbio Mine Reclamation Symposium https://doi.org/10.14288/1.0042484.

Muggeo, V.M.R., 2008. Segmented: an R package to fit regression models with broken-line relationships. R news 8, 20–25.

Mukundan, R., Pierson, D.C., Schneiderman, E.M., O'Donnell, D.M., Pradhanang, S.M., Zion, M.S., Matonse, A.H., 2013. Factors affecting storm event turbidity in a New York City water supply stream. CATENA 107, 80–88. https://doi.org/10.1016/j.catena.2013.02.002.

Nakamura, S., 1984. Soil Survey of American Samoa. United States Department of Agriculture, Soil Conservation Service and Department of Agriculture, Government of American Samoa, Washington, D.C.

Nathan, R.J., McMahon, T.A., 1990. Evaluation of automated techniques for base flow and recession analyses. Water Resour. Res. 26, 1465–1473. https://doi.org/10.1029/WR026i007p01465.

National Oceanic and Atmospheric Administration, 2023, Historical Hurrican Tracks, https://coast.noaa.gov/hurricanes, access date Aug 8, 2023.

Oleson, K.L.L., Falinski, K.A., Lecky, J., Rowe, C., Kappel, C.V., Selkoe, K.A., White, C., 2017. Upstream solutions to coral reef conservation: The payoffs of smart and cooperative decision-making. J. Environ. Manage. 191, 8–18. https://doi.org/10.1016/j.jenvman.2016.12.067.

Patterson, T.H. 1981. "Coastal and Inland Hydrology." In *Atlas of American Samoa*. Honolulu, Hawai'i: U.S. Office of Coastal Zone Management, American Samoa Government, and Dept of Geography, Univ. Hawai'i.

R Core Team, 2022. R: A Language and Environment for Statistical Computing. Austria, Vienna.

Ram, A.R., Terry, J.P., 2016. Stream turbidity responses to storm events in a pristine rainforest watershed on the Coral Coast of southern Fiji. Int. J. Sediment Res. 31, 279–290. https://doi.org/10.1016/j.ijsrc.2016.07.002.

Ramos-Scharrón, C.E., MacDonald, L.H., 2005. Measurement and Prediction of Sediment Production from Unpaved Roads, St John, US Virgin Islands. Earth Surface Processes and Landforms 30 (10), 1283–1304. https://doi.org/10.1002/esp.1201.

Rankl, J.G., 2004. Relations between Total-Sediment Load and Peak Discharge for Rainstorm Runoff on Five Ephemeral Streams in Wyoming. US Department of the Interior, US Geological Survey.

Reid, L.M., Dunne, T., 1984. Sediment Production from Forest Road Surfaces. Water Resources Research 20, 1753–1761. https://doi.org/10.1029/WR020i011p01753.

Rickson, R., 2014. Can control of soil erosion mitigate water pollution by sediments? Sci. Total Environ. 468–469, 1187–1197. https://doi.org/10.1016/j.scitotenv.2013.05.057.

Shuler, C.K., Dulai, H., Leta, O.T., Fackrell, J., Welch, E., El-Kadi, A.I., 2020. Understanding Surface Water-Groundwater Interaction, Submarine Groundwater Discharge, and Associated Nutrient Loading in a Small Tropical Island Watershed. Journal of Hydrology 585, 124342. https://doi.org/10.1016/j.jhydrol.2019.124342.

Stock, J.D., Rosener, M., Schmidt, K.M., Hanshaw, M.N., Brooks, B.A., Tribble, G., Jacobi, J., 2010. Sediment budget for a polluted Hawaiian reef using hillslope monitoring and process mapping. In: American Geophysical Union Fall Meeting. p. #EP22A-01.

Stock, J.D., Tribble, G.W., 2010. Erosion and sediment loads from two Hawaiian watersheds. In: Webb, J. (Ed.), 9th Federal Interagency Sedimentation Conference, Las Vegas. https://acwi.gov/sos/pubs/2ndJFIC/Contents/11D_Stock_02_28_10.pdf.

Storlazzi, C.D., Norris, B.K., Rosenberger, K.J., 2015. The influence of grain size, grain color, and suspended-sediment concentration on light attenuation: Why fine-grained terrestrial sediment is bad for coral reef ecosystems. Coral Reefs 34 (3), 967–975.

Syvitski, J.P.M., Vörösmarty, C.J., Kettner, A.J., Green, P., 2005. Impact of Humans on the Flux of Terrestrial Sediment to the Global Coastal Ocean. Science 308, 376–380. https://doi.org/10.1126/science.1109454.

Walling, D.E., Webb, B., 1982. Sediment availability and the prediction of storm-period sediment yields. Recent Dev. Explan. Predict. Eros. sediment yield 137, 327–337.

Walling, D.E., Webb, B.W., 1996. Erosion and Sediment Yield: A Global Overview. In: Erosion and Sediment Yield: Global and Regional Perspectives. Proceedings of the Exeter Symposium. IAHS Publ. no., 236.

Wolman, M.G., 1967. A Cycle of Sedimentation and Erosion in Urban River Channels". Geografiska Annaler: Series A, Physical Geography 49, 385–395. https://doi.org/10.1080/04353676.1967.11879766.

Ziegler, A.D., Benner, S.G., Tantasirin, C., Wood, S.H., Sutherland, R.A., Sidle, R.C., Jachowski, N., Nullet, M.A., Xi, L.X., Snidvongs, A., Giambelluca, T.W., Fox, J.M., 2014. Turbidity-based sediment monitoring in northern Thailand: Hysteresis, variability, and uncertainty. J. Hydrol. 519, 2020–2039. https://doi.org/10.1016/j.jhydrol.2014.09.010.